5564–5576 *Nucleic Acids Research, 2017, Vol. 45, No. 9* *Published online 28 February 2017*
doi: 10.1093/nar/gkx146

Structural characterization of interactions between transactivation domain 1 of the p65 subunit of NF-κB and transcription regulatory factors

Lauriane Lecoq, Luca Raiola, Philippe R. Chabot, Normand Cyr, Geneviève Arseneault, Pascale Legault and James G. Omichinski*

Department of Biochemistry and Molecular Medicine, Université de Montréal, Montréal, QC H3C 3J7, Canada

Received July 18, 2016; Revised February 15, 2017; Editorial Decision February 20, 2017; Accepted February 25, 2017

ABSTRACT

p65 is a member of the NF-κB family of transcriptional regulatory proteins that functions as the activating component of the p65–p50 heterodimer. Through its acidic transactivation domain (TAD), p65 has the capacity to form interactions with several different transcriptional regulatory proteins, including TFIIB, TFIIH, CREB-binding protein (CBP)/p300 and $TAF_{II}31$. Like other acidic TADs, the p65 TAD contains two subdomains ($p65_{TA1}$ and $p65_{TA2}$) that interact with different regulatory factors depending on the target gene. Despite its role in controlling numerous NF-κB target genes, there are no high-resolution structures of $p65_{TA1}$ bound to a target transcriptional regulatory factor. In this work, we characterize the interaction of $p65_{TA1}$ with two factors, the Tfb1/p62 subunit of TFIIH and the KIX domain of CBP. In these complexes, $p65_{TA1}$ transitions into a helical conformation that includes its characteristic ΦXXΦΦ motif (Φ = hydrophobic amino acid). Structural and functional studies demonstrate that the two binding interfaces are primarily stabilized by three hydrophobic amino acids within the ΦXXΦΦ motif and these residues are also crucial to its ability to activate transcription. Taken together, the results provide an atomic level description of how $p65_{TA1}$ is able to bind different transcriptional regulatory factors needed to activate NF-κB target genes.

INTRODUCTION

The NF-κB proteins are a family of transcription regulatory factors that control genes involved in a number of processes including the immune response, cell proliferation and cell survival (1). The five proteins that constitute the NF-κB family in mammals include p50, p52, p65 (also known as RelA), RelB and c-Rel. Members of the NF-κB family form different combinations of homo- and hetero-dimers with each other, and these various dimer combinations constitute the biologically active forms of the proteins, with the p65–p50 heterodimer being the most abundant cellular form. In unstressed cells, the various NF-κB dimers are predominantly sequestered in the cytoplasm, where they are maintained in a latent state through interactions with inhibitor of κB (IκB) proteins (2). In the canonical pathway, in response to a wide variety of stimuli such as stress or viral infections, the IκB protein is phosphorylated and this results in the rapid ubiquitination of the IκBα protein and its subsequent degradation via the ubiquitin-proteasome system. Following the degradation of the IκBα protein, the NF-κB dimer is released from its latent cytoplasmic state and translocated into the nucleus, where it activates transcription through its ability to specifically bind regulatory regions within target genes (3).

The p65 protein is the most thoroughly investigated of the five members of the NF-κB family, in part, because it is the activating component of the p65–p50 heterodimer. The p65 protein is essential for cell survival as p65 knockout cells are known to survive however p65 knockout mice do not, whereas this is not to be the case for other NF-κB family members, where functional redundancy has been observed in genetic studies (4). In response to different cellular signals, the p65 protein is transformed into one of its several active forms following a sequence of post-translational modifications that includes both phosphorylation and acetylation events (5). For example, it has been shown that phosphorylation of p65 on Ser276 results in a conformational change and this leads to enhanced binding to the histone acetyltransferase (HAT) CREB-binding protein(CBP)/p300 (6). The interaction with CBP leads to the acetylation of p65 at several positions and this acetylation is directly linked to enhanced transcriptional activity of p65 (7). In addition, several studies have identified other phosphorylation sites that appear to regulate the activity of p65 either by enhancing its acetylation or modify-

*To whom correspondence should be addressed. Tel: +1 514 343 6111; Fax: +1 514 343 2210; Email: jg.omichinski@umontreal.ca
Present address: Lauriane Lecoq, Molecular Microbiology and Structural Biology, UMR 5086 CNRS, Lyon 69007, France.

ing its ability to interact with other transcriptional regulatory factors (6,8–12). Based on these combined results, it appears that acetylation is required for maximal activity of p65, which is consistent with results showing that overexpression of CBP/p300 enhances the activation potential of p65 (7,13), whereas overexpression of histone deacetylases (HDAC) represses p65 activity (14).

In order to activate transcription of NF-κB target genes, p65 binds specifically to κB-binding sites present in either the enhancer or promoter regions of target genes. Like all members of the NF-κB family, the p65 protein contains a Rel homology domain (RHD) located near the amino-terminal region of the protein, which is responsible for both its ability to recognize specific DNA sequences on NF-κB regulated genes as well as to form heterodimers with other NF-κB-family members (2). Several crystal structures of the RHD of p65:p50 heterodimers bound to DNA sequences containing various NF-κB binding sites clearly demonstrate how the p65:p50 heterodimer is able to regulate a wide variety of target genes (15–17). In addition to the RHD, the p65 protein contains an acidic transactivation domain (TAD) located within the carboxyl-terminal 124 amino acids (residues 428–551 in the human p65 protein). The TAD is essential for the regulation of p65 target genes (18) and it functions by participating in a series of protein–protein interactions with a number of transcriptional regulatory proteins including HATs such as CBP/p300 (19), general transcription factors ($TAF_{II}31$, TFIIB, TFIID and TFIIH) (20–22) and chromatin remodeling complexes (23).

The TAD of p65 can be subdivided into two subdomains that are both capable of independently activating transcription of p65 regulated genes, and they are referred to as TA2, which is located between residues 428 and 521, and TA1, which is located between residues 521 and 551. Initial structural studies indicated that the full-length TAD of p65 (residues 428–551) was unstructured in the free form. This conclusion was based on the fact that homonuclear nuclear magnetic resonance (NMR) spectroscopy experiments demonstrated that the TAD of p65 displayed minimal chemical shift dispersion and was devoid of interproton nuclear Overhauser effects (NOEs) characteristic of helical structure. However, it was determined that addition of trifluoroethanol (TFE) to a fragment containing just the TA1 subdomain of the TAD of p65 induced changes characteristic of a helical conformation when analyzed using circular dichroism (CD) spectroscopy (24). Based on the presence of a TFE-induced helical conformation, it was suggested that the TAD of p65 adopts a helical conformation when bound to its partner proteins. This model is consistent with the fact that both the TA1 and TA2 subdomains of p65 contain consensus ΦXXΦΦ motifs (where Φ is a hydrophobic amino acid and X is any amino acid). This motif is present in numerous acidic TADs, including those of p53 and VP16, that transition from a predominantly disordered state to a helical conformation when bound to interacting domains of partner proteins such as CBP, $TAF_{II}31$, TFIIH and TFIIB (25–31). A recent NMR structure of the TA2 subdomain of p65 ($p65_{TA2}$, residues 425–490 of mouse p65) in complex with the TAZ1 domain of CBP demonstrated the importance of two ΦXXΦΦ motifs within TA2 for binding (32). In complex with TAZ1, four regions within $p65_{TA2}$ transition from an unstructured state into a helical conformation. Two of these helical regions encompass the ΦXXΦΦ motifs, and both motifs make important contributions to the binding interface of the complex.

Previous studies have shown that deletion of the TA1 subdomain of p65 ($p65_{TA1}$) results in the loss of ∼85% of its transactivation capacity (18). However, full transactivation activity is observed when $p65_{TA1}$ is tethered to a segment of p65 containing only the DNA-binding domain. Despite the importance of this domain in regulating the transcriptional activity of p65, there is currently no high-resolution structure of $p65_{TA1}$ bound to a transcriptional regulatory protein. Therefore, we have examined the interaction of $p65_{TA1}$ with two well-characterized targets of several other acidic TADs, the pleckstrin homology (PH) domain of the p62/Tfb1 (human/yeast) subunit of TFIIH ($p62_{PH}$/$Tfb1_{PH}$) and the KIX domain of CBP (CBP_{KIX}). We show that $p65_{TA1}$ binds to both $Tfb1_{PH}$ and CBP_{KIX} and adopts a similar α-helical conformation upon binding. In addition, we demonstrate that three hydrophobic residues within the ΦXXΦΦ motif of $p65_{TA1}$ play important roles in forming the binding interface with both $Tfb1_{PH}$ and CBP_{KIX} and that these residues are important to the ability of $p65_{TA1}$ to activate transcription. Taken together, the results provide detailed information on how $p65_{TA1}$ binds to two transcriptional regulatory factors that are required to help control the vast array of genes targeted by the NF-κB family.

MATERIALS AND METHODS

Cloning and purification of recombinant proteins

$Tfb1_{PH}$ (residues 1–115 of Tfb1) and $p62_{PH}$ (residues 1–108 of p62) were constructed as GST-fusion proteins and purified as previously described (33). CBP_{KIX} (residues 586–672) was cloned into a pET21a vector with a His-Tag and purified as previously described (34). The F612A/D622A/R624A/K667E quadruple CBP_{KIX} mutant (CBP_{KIX}-ΔMLL) and the Y650A/A654Q/Y658V triple CBP_{KIX} mutant (CBP_{KIX}-Δc-Myb) cloned into the pET21a vector encoding a His-Tag were generously provided by Dr Steven Smith (Queens University) and purified as previously described for the wild-type CBP_{KIX}. The $p65_{TA1}$ (residues 521–551) was cloned into the pET-His-GST-TEV vector generating a GST-fusion protein with an L523Y mutation to allow determination of peptide concentration at 280 nm. Mutations of $p65_{TA1}$ were carried out using the QuickChange II site-directed mutagenesis kit. GST-His–$p65_{TA1}$ and related mutants were grown in *Escherichia coli* host strain BL21(DE3) at 30°C and induced for 4 h in the presence of 1 mM Isopropyl β-D-1-thiogalactopyranoside (IPTG). The cells were lysed in 20 mM TRIS at pH 7.4 containing 1 M NaCl and 0.5 mM ethylenediaminetetraacetic acid, and bound to glutathione (GSH) resin (GE Healthcare). The GSH resin was washed first with lysis buffer and then with Tobacco Etch Virus (TEV) protease cleavage buffer. The $p65_{TA1}$ peptide was cleaved in batch from the resin overnight at room temperature in the presence of TEV protease. The resulting supernatant was then further purified on a Q-sepharose High-Performance column (GE Healthcare) equilibrated in 20

mM phosphate buffer at pH 6.5 and protein was eluted using a gradient of 20 mM $NaPO_4$ buffer at pH 6.5 containing 1 M NaCl. Purified protein was further dialyzed in suitable buffer for isothermal titration calorimetry (ITC) or NMR studies. For NMR experiments, $Tfb1_{PH}$, CBP_{KIX} and $p65_{TA1}$ were isotopically labeled by growth in minimal media containing ^{15}N-ammonium chloride (Sigma) and/or ^{13}C-glucose (Sigma) as the sole nitrogen and carbon sources.

Isothermal titration calorimetry studies

ITC titrations were performed at 25°C in 50 mM Tris–HCl buffer at pH 7.4 using a MicroCal VP-ITC system. Concentrations of injected $p65_{TA1}$ wild-type and mutant peptides in the syringe and $Tfb1_{PH}/p62_{PH}/CBP_{KIX}$ proteins in the cell varied respectively from 200 to 500 μM and from 20 to 50 μM, as determined by absorbance at 280 nm. Data were analyzed using MicroCal Origin Software and all experiments fit the single binding site model with 1:1 stoichiometry. Errors in K_D values were estimated from triplicate measurements or more.

NMR spectroscopy

NMR experiments were recorded at 25°C on Varian Unity Inova 500 and 600 MHz spectrometers. All NMR samples were prepared in 20 mM $NaPO_4$ buffer at pH 6.5 in either 10% D_2O/90%H_2O (v/v) or 100% D_2O. The $Tfb1_{PH}$–$p65_{TA1}$ complex was prepared using either 0.8 mM of ^{15}N-^{13}C $Tfb1_{PH}$ with two molar equivalents of unlabeled $p65_{TA1}$ or 0.8 mM of ^{15}N/^{13}C-$p65_{TA1}$ with two molar equivalents of unlabeled $Tfb1_{PH}$. The backbone and side chain resonances were assigned using 3D HNCO, HNCACB, HBCBCACONNH (35) and HCCH-TOCSY (36) experiments recorded on both complexes. Intramolecular distance restraints were extracted from 3D ^{15}N-edited NOESY-HSQC (37) and ^{13}C-edited HMQC-NOESY spectra (38), and intermolecular distance restraints were extracted from 3D ^{15}N-^{13}C F1-filtered, F3-edited NOESY experiments (39). All NOESY spectra for the complexes were recorded using a mixing time of 90 ms. Samples were exchanged three times in 100% D_2O before recording the ^{13}C-edited and the filtered NOESY spectra. In addition, HNCACB, HNCO and HCCONH experiments were recorded with 0.8 mM ^{15}N/^{13}C-$p65_{TA1}$ either in the absence or presence of two molar equivalents of CBP_{KIX} to extract chemical shifts for the secondary structure propensities (SSP) analyses. ^{13}C-edited HMQC-NOESY spectra in 100% D_2O were recorded at 25°C with a mixing time of 120 ms for the $p65_{TA1}$–CBP_{KIX} complex, and at 10°C with a mixing time of 350 ms for the free peptide. Resonance assignment of the CBP_{KIX}–$p65_{TA1}$ complex was performed using 3D HNCO, HNCACB, HBCBCACONNH and HCCH-TOCSY experiments on a 0.8 mM sample of ^{15}N/^{13}C-CBP_{KIX} with two molar equivalents of unlabeled $p65_{TA1}$. Intermolecular distance restraints for the $p65_{TA1}$–CBP_{KIX} complex were extracted from two 3D ^{15}N-^{13}C F1-filtered, F3-edited NOESY experiment, the first with ^{15}N/^{13}C-$p65_{TA1}$ in the presence of two molar equivalents of unlabeled CBP_{KIX} and the second with ^{15}N/^{13}C-CBP_{KIX} in the presence of two molar equivalents of unlabeled $p65_{TA1}$ in 100% D_2O. NMR data were processed with NMRPIPE (40) and analyzed with Analysis from the CCPNMR suite (41).

SSP analysis

SSP were assessed using SSP software (42) in $p65_{TA1}$ free form, bound to $Tfb1_{PH}$ and to CBP_{KIX}. Chemical shifts from $^{1}H_N$, $^{1}H_\alpha$, $^{15}N_H$, $^{13}C_\alpha$ and $^{13}C_\beta$ nuclei were used as input data and compared with random-coil chemical shift values from RefDB database (43).

Structural restraints and structure calculation

Backbone dihedral angles were obtained using either TALOSN for $Tfb1_{PH}$ (44) and TALOS+ (45), which gives more accurate predictions for $p65_{TA1}$. NOESY spectra were manually peaked and partially assigned. The NOE assignment was completed using ARIA2.3 (46), concomitantly with structure calculation. The ARIA program was run with eight iterations including twenty structures and a final iteration including 100 structures. The 20 best structures were subsequently refined in explicit water using CNS (47). Sidechain geometry was further optimized with the software YASARA (48) using the force field YASARA2 (49) and the SCWALL method (50). The Protein Structure Validation Suite was used to assess the overall quality of the structures (51). The figures of the structures were prepared using PyMol software (Warren Delano, http://www.pymol.org).

Yeast activation assays

DNA constructs encoding for $p65_{TA1}$ and its mutants were ligated into the PSH18–34 vector to produce fusion proteins with the DNA-binding domain of LexA. Yeast strains were transformed with the LexA operator-lacZ fusion proteins following a previously described protocol (52) and ß-galactosidase assays were performed as previously described (53). Results of the assays are presented as the mean of the percentage of ß-galactosidase units obtained for each of the tested LexA-fusion proteins. The activity of the LexA-GAL4 positive control is arbitrarily set to 100% for comparison with the other fusion proteins. The reported values are ± standard error of the mean obtained from a minimum of six independent experiments. Western blot analyses were performed with an anti-LexA antibody to verify equivalent expression of the LexA-fusion proteins.

RESULTS

TA1 from the p65 subunit of NF-κB binds to $Tfb1_{PH}/p62_{PH}$ and CBP_{KIX}

Based on amino acid sequence alignment (Supplementary Figure S1A and B), $p65_{TA1}$ contains a highly conserved region between residues 542 and 546 homologous to the ΦXXΦΦ motif that forms the recognition interface of several acidic TADs bound to their target proteins (54). Given that several of these acidic TADs have been shown to target both the PH domain present at the N-terminal of p62/Tfb1 subunit of the general transcription factor TFIIH

($p62_{PH}$/$Tfb1_{PH}$) and the KIX domain present in the histone acetyl transferase CBP (CBP_{KIX}), we attempted to examine the interaction of $p65_{TA1}$ with these two common targets of acidic TADs. Initially, we examined $p65_{TA1}$ binding to $Tfb1_{PH}$ and $p62_{PH}$ using ITC. The ITC experiments demonstrate that $p65_{TA1}$ binds to either $Tfb1_{PH}$ or $p62_{PH}$ with similar dissociation constants (K_D) of 15 ± 3 μM and 23 ± 4 μM, respectively, under the experimental conditions (Figure 1). Next, we examined whether or not $p65_{TA1}$ also binds to CBP_{KIX} using similar ITC experiments. Similar to $Tfb1_{PH}$ and $p62_{PH}$, CBP_{KIX} binds to $p65_{TA1}$ with a K_D of 15 ± 3 μM.

To further investigate these interactions, NMR chemical shift perturbation studies were performed to identify the binding site for $p65_{TA1}$ on both $Tfb1_{PH}$ and CBP_{KIX}. Addition of unlabeled $p65_{TA1}$ to either ^{15}N-labeled $Tfb1_{PH}$ or ^{15}N-labeled CBP_{KIX} results in significant changes in the ^{1}H and ^{15}N chemical shifts of the 2D ^{1}H-^{15}N HSQC spectrum and in both cases the binding of $p65_{TA1}$ occurs in fast-intermediate exchange on the NMR time scale (Figure 2A and B). In the case of $Tfb1_{PH}$, the signals that exhibited the most significant chemical shift changes in the HSQC spectrum following addition of $p65_{TA1}$(Supplementary Figure S2A), correspond to residues within the β5, β6 and β7 strands of the PH domain fold (Figure 2C). When mapped on the structure of $Tfb1_{PH}$, the binding site for $p65_{TA1}$ overlaps with the binding site of several other acidic TADs including those from p53 (27) and VP16 (29). In the experiments with CBP_{KIX}, the signals of CBP_{KIX} that exhibit the most significant chemical shift changes in the HSQC spectrum following addition of $p65_{TA1}$ (Supplementary Figure S2B), are associated with residues located in a groove formed by the C-terminal end of the α1 helix, the N-terminal end of the α2 helix and the C-terminal end of the α3 helix. When mapped on the structure of CBP_{KIX} (Figure 2D), the binding site for $p65_{TA1}$ appears to be similar to the binding site for the acidic TADs of the mixed lineage leukemia (MLL) protein (55) and the E-protein E2A (56).

NMR structure of the $Tfb1_{PH}$–$p65_{TA1}$ complex

To determine its structure in the bound state, we examined $p65_{TA1}$ in complex with $Tfb1_{PH}$ using NMR spectroscopy studies. The $Tfb1_{PH}$ was chosen for the NMR studies because it is considerable more stable than the $p62_{PH}$ protein over the long period of time required to collect the NMR data and it has served as a good model system for examining interactions with acidic TADs (27,29,33,34,57,58). The high-resolution NMR structure of the $Tfb1_{PH}$–$p65_{TA1}$ complex was calculated using 3447 NOE-derived distance restraints, 46 intermolecular NOEs and 211 dihedral angle restraints. The structure of the $Tfb1_{PH}$–$p65_{TA1}$ complex is well defined by the NMR data (Table 1). A total of 260 structures were calculated and the 20 lowest-energy structures are characterized by favorable backbone geometry, no significant violations of the experimental restraints and a pairwise root mean-square deviation (r.m.s.d.) of 0.3 Å for the backbone atoms and 0.8 Å for heavy atoms (Table 1). In complex with $p65_{TA1}$, the structure of $Tfb1_{PH}$ (Figure 3) is similar to its structure in the unbound form (33), which consists of a PH-domain fold containing a seven-stranded β sandwich (β1–β7) followed by a single α-helix (α1). In complex with $Tfb1_{PH}$, $p65_{TA1}$ forms a 13-residue α-helix (Figure 3) between F534 and L546, and the helix forms the interface with $Tfb1_{PH}$.

$Tfb1_{PH}$–$p65_{TA1}$ binding interface

The key residues of $p65_{TA1}$ at the interface with $Tfb1_{PH}$ are three hydrophobic residues (F542, L545 and L546) located within the ΦXXΦΦ motif. In the structure of the complex, the side chain of F542 from $p65_{TA1}$ is fully buried in a pocket formed by Q49, A50, T51, K57, M59, R61 and M88 of $Tfb1_{PH}$ (Figure 4A). In this pocket, one side of the aromatic ring of F542 is in position to form an amine-π interaction with the side chain of Q49. In addition, the other side of the aromatic ring of F542 has the potential to form either a cation-π interactions with K57 of $Tfb1_{PH}$ or a sulfur–π interaction with M59 of $Tfb1_{PH}$. This is based on the fact that the positive charge of K57 occurs at a distance between 5 and 9 Å from the center of the aromatic ring of F542 and the sulfur atom of M59 occurs at a distance between 5 and 7 Å from the center of the aromatic ring of F542 in the 20 NMR structures of the $p65_{TA1}$–$Tfb1_{PH}$ complex. Although F542 of p65 seems to be the most crucial residue at the interface with $Tfb1_{PH}$, L545 and L546 from the ΦXXΦΦ motif in $p65_{TA1}$ also appear to contribute to the overall binding energy. These two leucine residues are located at the extreme C-terminal end of the $p65_{TA1}$ helix, where L545 is inserted into a pocket formed by P52, S55 and K57, whereas L546 appears to form van der Waals contacts with the side chain of Q49 from $Tfb1_{PH}$ (Figure 4B). In addition to the interactions involving hydrophobic residues from the ΦXXΦΦ motif in $p65_{TA1}$, the structures suggest two possible electrostatic interactions between negatively charged residues of $p65_{TA1}$ and positively charged residues of $Tfb1_{PH}$ (Supplementary Figure S3). The first one occurs between D539 from $p65_{TA1}$ and either R61 or R86 of $Tfb1_{PH}$, and a second one occurs between D541 of $p65_{TA1}$ and K57 of $Tfb1_{PH}$.

$p65_{TA1}$ α-helical propensity depends on substrate presence

Our structure of the $Tfb1_{PH}$–$p65_{TA1}$ complex reveals that $p65_{TA1}$ forms a 13-residue α-helix between residues 534 and 546 in complex with $Tfb1_{PH}$ and this suggests that a significant conformational change occurs between the unbound and the bound states based on earlier NMR studies with the free $p65_{TA1}$. Given the recent advances in the identification of protein secondary structure elements based on NMR chemical shifts values (59), we decided to reinvestigate the α-helical propensity of $p65_{TA1}$ in the free form as well as to determine if $p65_{TA1}$ forms a similar α-helix in complex with CBP_{KIX}. For these studies, we performed NMR experiments to obtain the complete ^{1}H, ^{15}N and ^{13}C chemical shift assignment for ^{15}N/^{13}C-labeled $p65_{TA1}$ in the free state and bound to CBP_{KIX} and compared them with the values obtained for the complex with $Tfb1_{PH}$ (Supplementary Figure S4). The SSP of $p65_{TA1}$ in the free state, bound to $Tfb1_{PH}$ as well as bound to CBP_{KIX} were determined using the SSP software (42). For the SSP analysis, $^{1}H_N$, $^{1}H_\alpha$, $^{15}N_H$, $^{13}C_\alpha$ and $^{13}C_\beta$ chemical shift values of $p65_{TA1}$ were used as the input data. The SSP predictions indicate that $p65_{TA1}$ displays

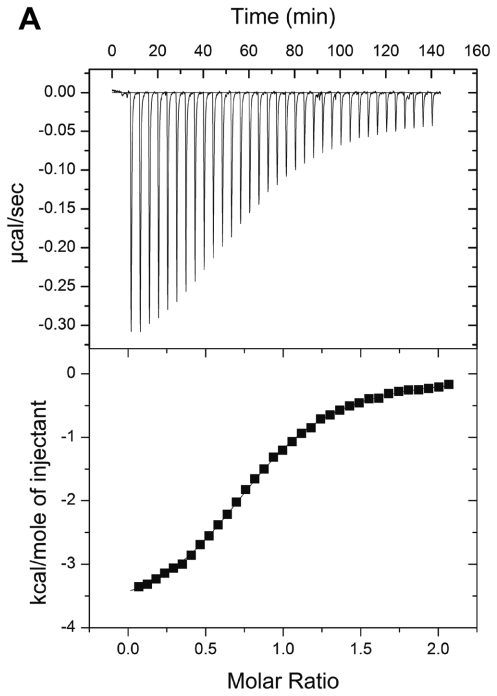

B

Kd (μM)	$p65_{TA1}$
$p62_{PH}$ WT	23 ± 4
$Tfb1_{PH}$ WT	15 ± 3
CBP_{KIX} WT	15 ± 3
CBP_{KIX} Δc-Myb	13 ± 2
CBP_{KIX} ΔMLL	ND*

*ND: no heat detected

C

Kd (μM)	$Tfb1_{PH}$	CBP_{KIX}
$p65_{TA1}$ WT	15 ± 3	15 ± 3
$p65_{TA1}$ F542A	ND	ND
$p65_{TA1}$ L545A	24 ± 2	29 ± 5
$p65_{TA1}$ L546A	21 ± 1	31 ± 5

Figure 1. Binding of $p65_{TA1}$ to $Tfb1_{PH}/p62_{PH}$ and CBP_{KIX} characterized by ITC. (**A**) Representative ITC thermogram obtained by successive additions of $p65_{TA1}$ to $Tfb1_{PH}$. (**B**) Summary of dissociation constants (K_D) values obtained from ITC experiments of $p65_{TA1}$ with $p62_{PH}$, $Tfb1_{PH}$, CBP_{KIX} and CBP_{KIX} mutants. (**C**) Summary of K_D values obtained from ITC experiments for $Tfb1_{PH}$ and CBP_{KIX} with $p65_{TA1}$ mutants from the ΦXXΦΦ motif.

Table 1. NMR and refinement statistics for the $Tfb1_{PH}$–$p65_{TA1}$ complex (PDB ID: 5URN)

NMR distance and dihedral constraints	$Tfb1_{PH}$	$p65_{TA1}$
Number of distance constraints		
Total intramolecular NOEs	3066	381
Intra-residue	914	252
Inter-residue		
Sequential (|i-j| = 1)	544	86
Medium-range (2< = |i-j|< = 4)	361	43
Long-range (|i-j|>5)	905	0
Total intermolecular NOEs	46	
Total dihedral angle restraints		
φ	94	12
ψ	93	12
Structure statistics	**$Tfb1_{PH}$–$p65_{TA1}$**	
Global quality scores (raw/*Z*-score)		
Verify 3D	0.29/−2.73	
ProsaII (-ve)	0.43/−0.91	
Procheck (φ/ψ only)	−0.53/−0.77	
Procheck (all dihedral angles)	−0.27/−1.60	
MolProbity clashscore	20.77/−2.04	
Violations (mean and s.d.)		
Distance constraints (Å)	0.041 ± 0.002	
Dihedral angle constraints (°)	1.56 ± 0.03	
Deviations from idealized geometry		
Bond lengths (Å)	0.0080 ± 0.0001	
Bond angles (°)	0.78 ± 0.01	
Atomic pairwise coordinate RMSD[a] (Å)		
Heavy atoms	0.8 ± 0.1	
Backbone atoms	0.3 ± 0.1	
Ramachandran statistics[a] (%)		
Residues in most favored regions	92.7	
Residues in additional allowed regions	6.7	
Residues in generously allowed regions	0.6	
Residues in disallowed regions	0.0	

[a]Pairwise r.m.s. deviation and Ramachandran statistics were calculated among 20 structures refined in water for residues 4–63 and 86–112 of $Tfb1_{PH}$ and residues 534–546 of $p65_{TA1}$.

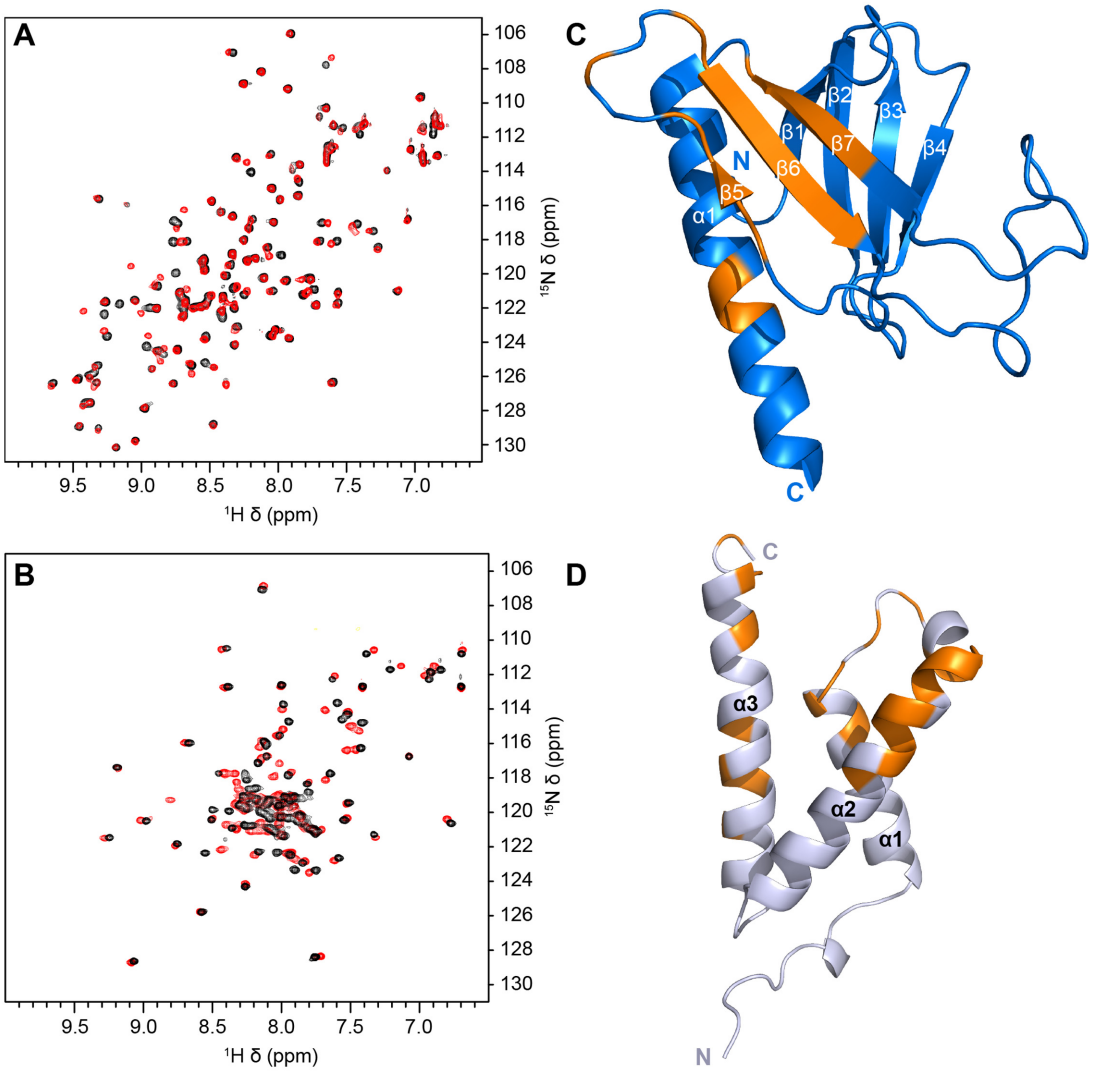

Figure 2. Nuclear magnetic resonance (NMR) spectra of $p65_{TA1}$ binding to $Tfb1_{PH}$ and CBP_{KIX}. (**A** and **B**) Overlay of the 2D ^{1}H-^{15}N-HSQC NMR spectra of ^{15}N-$Tfb1_{PH}$ (**A**) and ^{15}N-CBP_{KIX} (**B**) either in the absence (black) or in the presence (red) of two equivalents of $p65_{TA1}$. (**C**) Residues that undergo significant chemical shift perturbations (>0.05 ppm) in the 2D ^{1}H-^{15}N HSQC spectrum upon addition of $p65_{TA1}$ to ^{15}N-labeled $Tfb1_{PH}$ are mapped in orange onto the structure of free $Tfb1_{PH}$ (in blue, PDB ID: 1Y5O (33)). (**D**) Residues that undergo significant chemical shift perturbations (>0.1 ppm) in the 2D ^{1}H-^{15}N HSQC spectrum upon addition of $p65_{TA1}$ to ^{15}N-labeled CBP_{KIX} are mapped in orange onto the structure of CBP_{KIX} (in silver, PDB ID: 2AGH (55)).

helical propensity for the residues within the ΦXXΦΦ motif in the free form, and that this helical propensity is accentuated when it is bound to either $Tfb1_{PH}$ or CBP_{KIX} (Figure 5).

To further investigate the helical propensity of $p65_{TA1}$ in the unbound state, a series of 3D ^{13}C-NOESY-HMQC experiments were conducted with $^{15}N/^{13}C$-labeled $p65_{TA1}$. The initial experiments were recorded at 25°C and no NOE signals were observed using mixing times of either 90 and 180 ms. In subsequent experiments, the temperature was lowered to 10°C to decrease the molecular tumbling rate of $p65_{TA1}$ and the mixing time was increased to 350 ms. At 10°C, the chemical shift values of the free $p65_{TA1}$ did not change significantly after taking into account the global chemical shift displacement due to the temperature change, and this suggests that the conformation of $p65_{TA1}$ did not change dramatically as a result of the change in temperature. At this lower temperature, NOE signals indicative of a helical conformation are present between the H_{α} and the $H_{\beta i+3}$ for the H_{α} signals F542, S543 and A544 of $p65_{TA1}$. The presence of these medium range NOE signals correlate with the SSP results and suggests there is a short transient helical conformation in the free form that involves residues within the ΦXXΦΦ motif of $p65_{TA1}$.

Localization of the $p65_{TA1}$-binding site on CBP_{KIX}

CBP_{KIX} contains two distinct binding sites that are recognized by acidic TADs and these two sites are referred to as the 'MLL-binding site' and the 'c-Myb-binding site' (60–62). The MLL-binding site is located at the interface where helices α1, α2 and α3 of CBP_{KIX} converge, whereas the c-Myb-binding site is located on the opposite face in

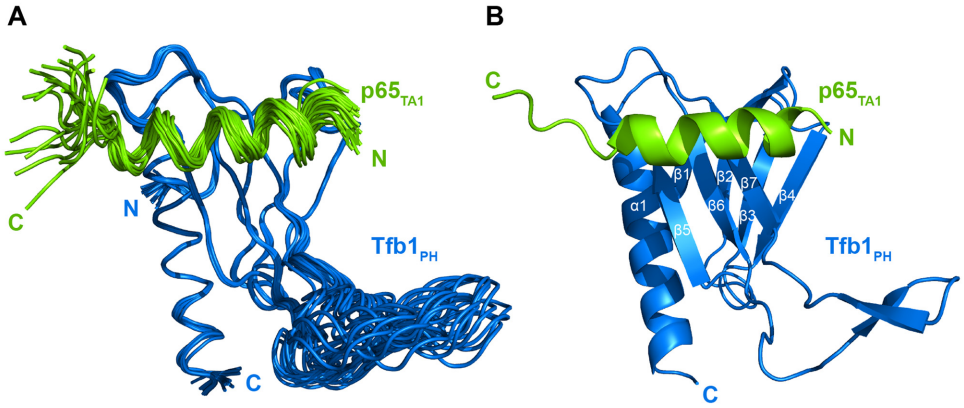

Figure 3. NMR structure of the $Tfb1_{PH}$–$p65_{TA1}$ complex. (**A**) Overlay of the 20 NMR structures of the $Tfb1_{PH}$–$p65_{TA1}$ complex. The structures of $Tfb1_{PH}$ (blue) and $p65_{TA1}$ (chartreuse) are displayed in the coil representation. For clarity, only residues 533–551 of $p65_{TA1}$ are shown. (**B**) Ribbon representation of the lowest-energy structure of the $Tfb1_{PH}$–$p65_{TA1}$ complex with $Tfb1_{PH}$ and $p65_{TA1}$ colored as in **A**. Secondary structure elements are indicated on $Tfb1_{PH}$. The α-helix of $p65_{TA1}$ includes residues F534 to L546.

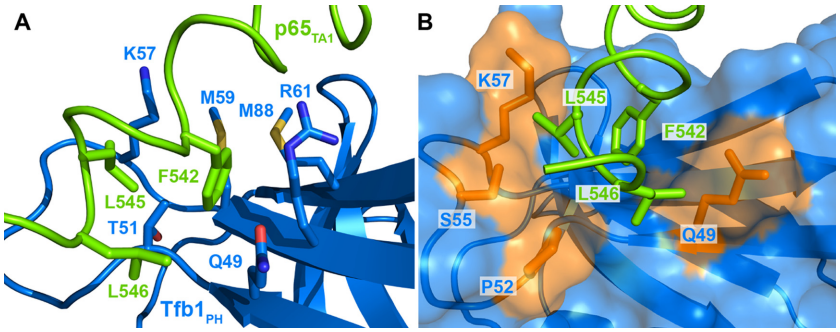

Figure 4. Close up of key residues forming the binding interface in the $Tfb1_{PH}$–$p65_{TA1}$ complex. (**A**) The structures of $p65_{TA1}$ (in chartreuse) and $Tfb1_{PH}$ (in marine) are shown in ribbon representations with the side chains of the key residues at the interface in stick representations. F542 of $p65_{TA1}$ is in position to form an amine–π interaction with Q49 as well as either a cation–π with K57 or a sulfur–π interaction with M59 of $Tfb1_{PH}$. In addition, the methyl group of L545 from $p65_{TA1}$ is in close proximity to the methyl group of T51 of $Tfb1_{PH}$. (**B**) In this second orientation where $Tfb1_{PH}$ is shown as a surface representation, the methyl groups of L545 and L546 of $p65_{TA1}$ are buried in hydrophobic pockets on the surface of $Tfb1_{PH}$. The side chains of the key residues forming the interface from $Tfb1_{PH}$ in close proximity to L545 and L546 are colored in orange and include Q49, P52, S55 and K57.

a hydrophobic groove created by the α3 helix. To verify that the MLL-binding site is in fact the preferred binding site as suggested by the NMR chemical shift perturbation studies, two previously described mutants of CBP_{KIX} [CBP_{KIX}-ΔMLL (F612A/D622A/R624A/K667E quadruple mutant) and CBP_{KIX}-Δc-Myb (Y650A/A654Q/Y658V triple mutant)] were prepared and their binding to $p65_{TA1}$ determined by ITC. The ITC experiments demonstrate that $p65_{TA1}$ binds to CBP_{KIX}-Δc-Myb mutant with a K_D of 13 ± 2 μM, which is virtually identical to the binding observed with wild-type CBP_{KIX} (Figure 1A and B). In contrast, no significant heat change is observed for $p65_{TA1}$ binding to the CBP_{KIX}-ΔMLL mutant and this indicates that the affinity for $p65_{TA1}$ has decreased by at least two orders of magnitude. Thus, the ITC results with the CBP_{KIX} binding site mutants are in agreement with the NMR chemical shift perturbation studies (Figure 2D) and support the fact that $p65_{TA1}$ preferentially binds to the MLL-binding site of CBP_{KIX}.

NMR structure of the CBP_{KIX}–$p65_{TA1}$ complex

The interaction of $p65_{TA1}$ with CBP_{KIX} was further investigated by high resolution NMR spectroscopy to determine a structure of the CBP_{KIX}–$p65_{TA1}$ complex. A total of 37 intermolecular NOE restraints were incorporated into the calculations to define the orientation of $p65_{TA1}$ toward CBP_{KIX}. The residues of CBP_{KIX} involved in the intermolecular NOEs are all located either in the cleft formed at the junction of the three helices (I611, F612, A619) or on the surface of the α2 and α3 helices (R624, M625, N627, L628, Y631 on α2; I660 and L664 on α3). The structure of the CBP_{KIX}–$p65_{TA1}$ complex displays good structural statistics (Table 2) and it resembles the structures of several other acidic TADs bound to CBP_{KIX} including MLL (55) and E2A (56) (Figure 6A–C). Consistent with the SSP results, $p65_{TA1}$ forms a 17-residue helix between F534 and S550 when bound to CBP_{KIX}. The predominant determinants for forming the $p65_{TA1}$–CBP_{KIX} interface come from contacts involving hydrophobic residues along almost the entire length of the $p65_{TA1}$ helix (F534, I537, A538, F542, L545 and L546), which is anchored onto CBP_{KIX} (Figure 6D). The first contacts occur between residues in the N-

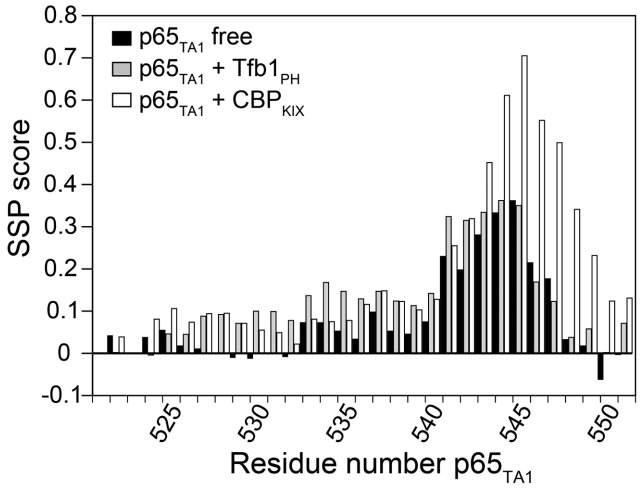

Figure 5. Helical propensity of $p65_{TA1}$ in the free form as well as in complex with $Tfb1_{PH}$ and CBP $_{KIX}$. The secondary structure propensities (SSP) were determined based on the ^{15}N, $^{1}H_N$, $^{13}C\alpha$, $^{13}C\beta$ and $^{1}H\alpha$ chemical shifts of $p65_{TA1}$. The values were derived using chemical shifts determined from NMR experiments with $p65_{TA1}$ in the unbound state (black) as well as in complex with either $Tfb1_{PH}$ (gray) or CBP_{KIX} (white). Positive values represent a propensity to form α-helical secondary structure and negative values represent β-strand structure propensity.

terminal part of the $p65_{TA1}$ helix and the α2 and α3 helices of CBP_{KIX}. In particular, the phenyl ring of F534 from $p65_{TA1}$ is in position to form a π-π stacking interaction with the phenol ring of Y631 from CBP_{KIX}, whereas the methyl group of A538 is positioned near the methyl groups of I611, L628 and I660. In addition, there are several interactions involving the three hydrophobic residues from the ΦXXΦΦ motif (F542, L545 and L546). These three residues of $p65_{TA1}$ are buried in a deep hydrophobic cleft on the surface of CBP_{KIX} formed by the three helices. In the structure, they are positioned to be in close contact with F612, A619, M625, L664 and R668 of CBP_{KIX}. Although interactions involving the hydrophobic residues in the $p65_{TA1}$ helix appear to be the driving force for binding to CBP_{KIX}, the structure suggests that electrostatic interactions involving negatively charged amino acids of p65 and positively charged residues of CBP are also important for forming the binding interface (Figure 6E). More specifically, D539 and D541 of $p65_{TA1}$ are in position to form an electrostatic interaction with the ammonium group of K667 and the guanidinium group of R624 of CBP_{KIX}, respectively. Thus, the structure demonstrates that the binding of $p65_{TA1}$ to CBP_{KIX} involves a combination of hydrophobic and electrostatic interactions and this is consistent with what has been observed for other acidic TADs binding to CBP_{KIX}.

F542 of the ΦXXΦΦ motif in $p65_{TA1}$ is crucial for binding to $Tfb1_{PH}$ and CBP_{KIX}

To quantitatively investigate the contribution of the hydrophobic residues within the ΦXXΦΦ motif of $p65_{TA1}$ for binding to CBP_{KIX} and $Tfb1_{PH}$, we prepared mutants of $p65_{TA1}$ where the three hydrophobic residues were substituted with alanine (F542A, L545A and L546A) for evaluation by ITC (Figure 1C). Under the ITC conditions, no significant heat change is observed for the binding of the F542A mutant of $p65_{TA1}$ with either $Tfb1_{PH}$ or CBP_{KIX} and this indicates that the affinity of the $p65_{TA1}$ F542A mutant has decreased by at least two orders of magnitude in both cases. The results with the F542A mutant are in agreement with our NMR structural data demonstrating that F542 of $p65_{TA1}$ is a key component of the interface in both the $p65_{TA1}$–$Tfb1_{PH}$ and the $p65_{TA1}$–CBP_{KIX} complexes. In the case of the L545A and L546A mutants of $p65_{TA1}$, the effect of the alanine substitution on $p65_{TA1}$ binding to either $Tfb1_{PH}$ or CBP_{KIX} is less dramatic, with the two mutants displaying approximately a 1.5-fold decrease in affinity for both $Tfb1_{PH}$ and CBP_{KIX} (Figure 1C). Consistent with the NMR structures, the ITC studies indicate that F542 within the ΦXXΦΦ motif is a key residue required for $p65_{TA1}$ binding to both $Tfb1_{PH}$ and CBP_{KIX}.

$p65_{TA1}$ interaction with $Tfb1_{PH}$ and CBP_{KIX} correlates with transcriptional activity

Previous studies have shown that the full activation of several NF-κB-regulated genes depends on the presence of $p65_{TA1}$ and that F542 within the ΦXXΦΦ motif is essential for this activity (20). To test the relative importance of the hydrophobic residues in the ΦXXΦΦ motif on the transcriptional activation associated with $p65_{TA1}$, we examined the relative activities of the F542A, L545A and L546A mutants of $p65_{TA1}$ in a yeast model system. The yeast system has been previously used to characterize the activity of both $p65_{TA1}$ and $p65_{TA2}$ and it provides a good correlation to what has been observed in human cells (20,24). For these studies, $p65_{TA1}$ and the mutants were fused to the DNA-binding domain of LexA ($LexA_{DBD}$) in order to measure their relative ability to activate transcription from a *lacZ* reporter gene. For the comparison, a $LexA_{DBD}$–GAL4 fusion protein served as a positive control (100% activity), whereas the $LexA_{DBD}$ protein served as a negative control (no activity). In yeast, $LexA_{DBD}$–$p65_{TA1}$ activates transcription at a level similar (96 ± 6%) to $LexA_{DBD}$–GAL4 (Figure 7), whereas the $LexA_{DBD}$–$p65_{TA1}$ F542A mutant is almost completely devoid of activity (4.3 ± 3%). In addition, both the $LexA_{DBD}$–$p65_{TA1}$ L545A and $LexA_{DBD}$–$p65_{TA1}$ L546A mutants also display a reduced ability to activate transcription (47 ± 5 and 27 ± 6%, respectively), but the decrease is less dramatic than that observed with the F542A mutant. These findings are consistent with both the NMR and ITC studies, which demonstrate the important role of the three hydrophobic residues within the ΦXXΦΦ motif of $p65_{TA1}$ for transcriptional activation.

DISCUSSION

Like several other acidic TADs, the TAD of p65 contains two distinct subdomains and both subdomains have been shown to be capable of independently activating transcription of select NF-κB target genes. Given the vast array of genes regulated by the p65–p50 heterodimer, it appears that the two subdomains interact with different transcriptional regulatory targets depending on the target gene being activated. In this study, we have characterized

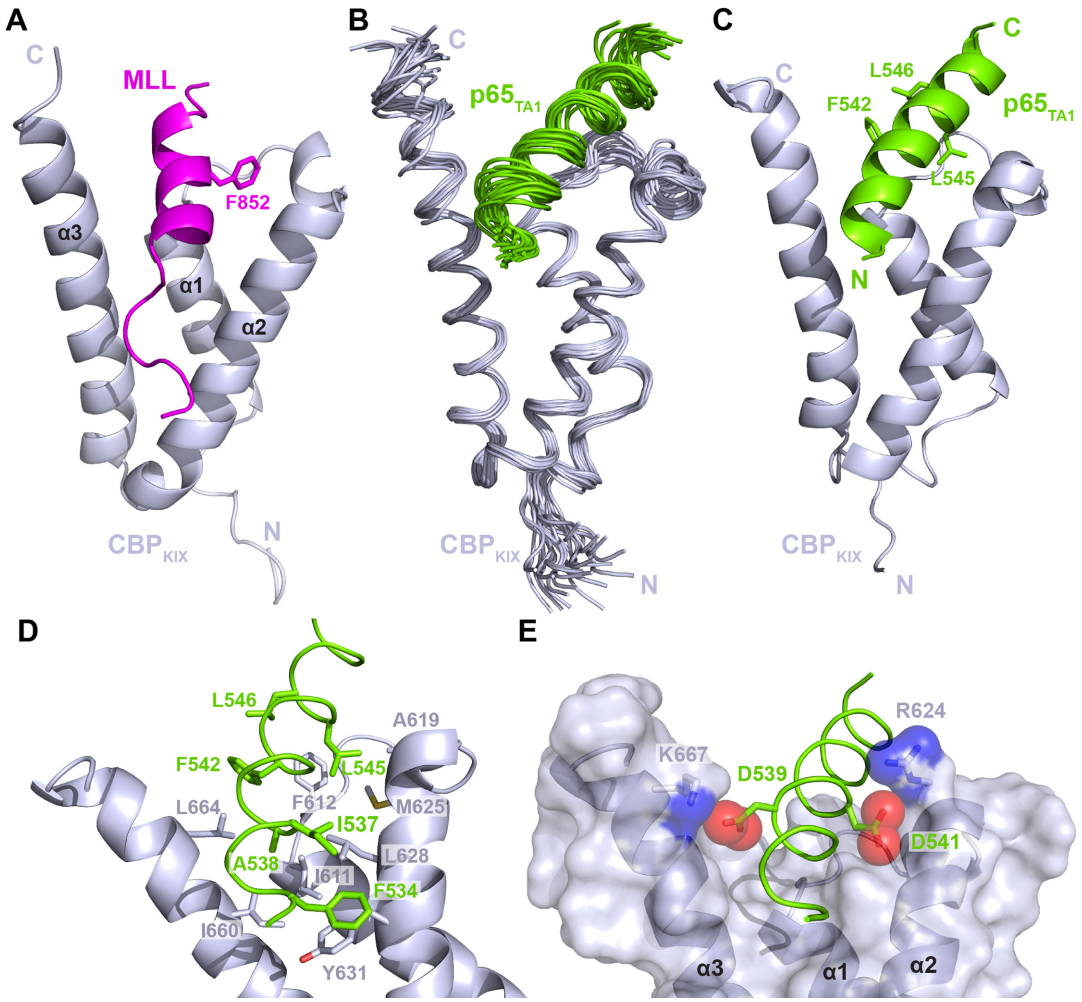

Figure 6. $p65_{TA1}$ interacts with CBP_{KIX} in the same binding-site as MLL. (**A**) Cartoon representation of CBP_{KIX} (gray) in complex with the MLL peptide [PDB ID : 2LXS (61)]. The key residue F852 of MLL is shown as sticks. (**B**) Overlay of the 20 NMR structures of the CBP_{KIX}–$p65_{TA1}$ complex. The structures of CBP_{KIX} (gray) and $p65_{TA1}$ (chartreuse) are displayed in the coil representation. For clarity and for comparison with the $Tfb1_{PH}$–$p65_{TA1}$ complex, residues 533 to 551 of $p65_{TA1}$ are shown. (**C**) Ribbon representation of the lowest-energy structure of the CBP_{KIX}–$p65_{TA1}$ complex. The three hydrophobic residues from the ΦXXΦΦ motif of $p65_{TA1}$ (F542, L545 and L546) are represented in stick form. (**D**) Close-up view of key interactions at the interface of the CBP_{KIX}–$p65_{TA1}$ complex. Several residues in both domains contribute to anchor $p65_{TA1}$ in the cleft created at the junction of the three helices of CBP_{KIX}. (**E**) Close-up view on electrostatic interaction between D539 of $p65_{TA1}$ and K667 of CBP_{KIX}, and between D541 of $p65_{TA1}$ and R624 of CBP_{KIX}.

the interaction of the TA1 subdomain from the TAD of p65 ($p65_{TA1}$) with two well-characterized targets of acidic TADs, the PH domain from the Tfb1/p62 ($Tfb1_{PH}/p62_{PH}$) subunit of TFIIH and the KIX domain of CBP (CBP_{KIX}). ITC experiments demonstrate that $p65_{TA1}$ binds to both $p62_{PH}/Tfb1_{PH}$ and CBP_{KIX}, and NMR structural studies show that binding to both of these transcriptional regulatory proteins stabilizes an α-helical structure in $p65_{TA1}$ that is centered around the ΦXXΦΦ motif located between Phe542 and Leu546. The structure of the $p65_{TA1}$–$Tfb1_{PH}$ complex clearly demonstrates that the three hydrophobic residues within the ΦXXΦΦ motif of $p65_{TA1}$ (Phe542, Leu545 and Leu546) all play important roles at the binding interface with $Tfb1_{PH}$. Consistent with what is observed in the $Tfb1_{PH}$–$p65_{TA1}$ complex, these same three residues also make key interactions at the interface with CBP_{KIX} in the NMR structure of the $p65_{TA1}$–CBP_{KIX} complex. The binding interface is also complemented by electrostatic interactions involving negatively charged amino acids from the helical region of $p65_{TA1}$ (D539 and D541) and positive charged amino acids from either $Tfb1_{PH}$ or CBP_{KIX}. In addition, we demonstrate that the three hydrophobic residues from the ΦXXΦΦ motif are important for transcriptional activation in a yeast model system, which suggests that these residues play a key role in regulating a number of genes activated by p65 through interactions with transcription regulatory factors such as TFIIH and CBP.

The presence of two independent subdomains within the acidic TAD of p65 is similar to what has been observed in a number of other mammalian transcriptional regulatory factors including p53 (63), VP16 (64), FOX03a (65) and EKLF (66). Two key elements link these acidic TADs from different transcriptional regulators to their function: an abundance of negatively charged amino acids through-

Table 2. NMR and refinement statistics for the CBP_{KIX}–$p65_{TA1}$ complex (PDB ID: 5U4K)

NMR distance and dihedral constraints	CBP_{KIX}	$p65_{TA1}$
Number of distance constraints		
Total intramolecular NOEs	1006	333
Intra-residue	631	226
Inter-residue		
Sequential (|i-j| = 1)	141	75
Medium-range (2< = |i-j|< = 4)	133	32
Long-range (|i-j|>5)	101	0
Total intermolecular NOEs	37	
Total dihedral angle restraints		
φ	82	18
ψ	82	19
Structure statistics	**CBP_{KIX}–$p65_{TA1}$**	
Global quality scores (raw/*Z*-score)		
Verify 3D	0.30/−2.57	
ProsaII (-ve)	0.69/0.17	
Procheck (φ/ψ only)	−0.10/−0.08	
Procheck (all dihedral angles)	0.01/0.06	
MolProbity Clashscore	11.25/−0.40	
Violations (mean and s.d.)		
Distance constraints (Å)	0.060 ± 0.006	
Dihedral angle constraints (°)	0.49 ± 0.08	
Deviations from idealized geometry		
Bond lengths (Å)	0.0078 ± 0.0001	
Bond angles (°)	0.73 ± 0.02	
Atomic pairwise coordinate RMSD[a] (Å)		
Heavy atoms	1.1 ± 0.1	
Backbone atoms	0.6 ± 0.1	
Ramachandran statistics[a] (%)		
Residues in most favored regions	99.3	
Residues in additional allowed regions	0.7	
Residues in generously allowed regions	0.0	
Residues in disallowed regions	0.0	

[a]Pairwise r.m.s. deviation and Ramachandran statistics were calculated among 20 structures refined in water for residues 587–672 of CBP_{KIX} and residues 534–550 of $p65_{TA1}$.

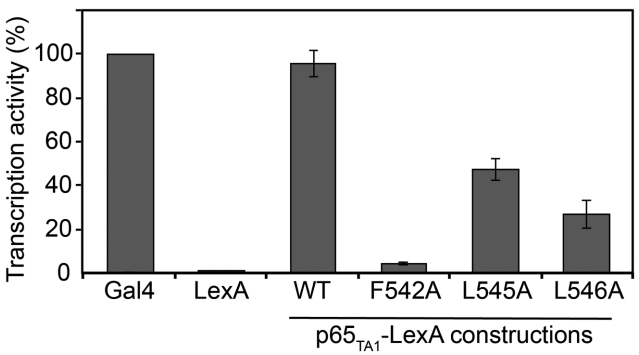

Figure 7. Identification of key residues required for $p65_{TA1}$ transactivation. LexA-fusion proteins of $p65_{TA1}$ and mutants were co-expressed in yeast with the reporter for the LexA operator-Lac-Z fusion plasmid pSH18–34. The percentage of activity for each fusion proteins is shown relatively to the positive control LexA-GAL4 (474–881), which was set to a maximum of activity (100%). Data represent mean and standard deviation obtained over at least six independent experiments.

out the entire length of the sequence and the presence of a ΦXXΦΦ motif. Typically, acidic TADs are intrinsically disordered in their unbound states, but adopt a more ordered structure in the bound state. In most complexes examined to date, the bound structure consists of a mainly alpha helical conformation, although examples of extended structures have also been reported (31,32,56,60–62,67–72). Like other acidic TADs, initial NMR studies indicated that the full-length TAD of p65 was intrinsically disordered in the unbound form, but it was predicted to adopt a helical conformation when bound to target proteins with hydrophobic residues from the ΦXXΦΦ motifs being key contributors to the binding interface (24). The NMR structure of the $p65_{TA2}$ subdomain bound to the TAZ1 domain of CBP clearly supports these earlier predictions (19). In complex with CBP_{TAZ1}, $p65_{TA2}$ adopts four distinct helical regions and two of these regions contain ΦXXΦΦ motifs that provide important contacts at the binding interface. Our current studies with the $p65_{TA1}$–$Tfb1_{PH}$ and $p65_{TA1}$–CBP_{KIX} complexes are also in agreement with these earlier predictions and again highlight the importance of the ΦXXΦΦ motif in formation of the binding interface with $p65_{TA1}$. However, the current NMR studies with $p65_{TA1}$ indicate that the ΦXXΦΦ motif transiently adopts a short helical conformation even in the unbound state, and that a longer helical conformation is stabilized upon binding to target factors such as CBP_{KIX} and $Tfb1_{PH}$. Thus, the two complexes containing $p65_{TA1}$ highlight how this domain alters its conformation so that it is able to bind to different targets in order to specifically activate transcription of p65–p50 target genes.

Several other structures of CBP_{KIX} or $p62_{PH}$/$Tfb1_{PH}$ have been determined previously in complex with acidic TADs from different transcriptional regulatory factors. In each complex containing CBP_{KIX}, the acidic TADs have been shown to transition from a predominantly disordered conformation in the unbound state to a helical conformation in the bound state (61,62,69). These previous structures also indicated the presence of two distinct binding sites on the surface of CBP_{KIX}, the so called MLL and c-Myb sites, and that TADs can bind independently to one site or in a cooperative manner to both sites (60,73). For

example, the two subdomains from the TAD of FOXO3a can bind to CBP_{KIX} either as individual subdomains to one of the sites or in a cooperative manner to both sites as the full-length TAD (68). In contrast, there is a single binding site for acidic TAD on the surface of $Tfb1_{PH}/p62_{PH}$ that is formed by the β5, β6 and β7 strands of the PH domain. However, TAD binding to $Tfb1_{PH}/p62_{PH}$ has been shown to occur in either a helical conformation or an extended conformation depending on the TAD (27,29,31,57,58). Our structural studies demonstrate that $p65_{TA1}$ binds to both CBP_{KIX} and $Tfb1_{PH}$ in a similar manner using a similar helical conformation. The main difference between $p65_{TA1}$ in the two complexes appears to be at the C-terminus of the helix, where the last residue of the helix is L546 in the $Tfb1_{PH}$ complex compared with S550 in the CBP_{KIX} complex. Our NMR studies together with mutational studies indicate that only one molecule of $p65_{TA1}$ binds to CBP_{KIX} at the MLL-binding site. The $p65_{TA1}$ helix covers 763 $Å^2$ on the surface of CBP_{KIX}, but only 479 $Å^2$ on the surface of $Tfb1_{PH}$. This difference in size of the binding interfaces is consistent with the fact that $p65_{TA1}$ forms a longer helix when bound to CBP_{KIX} than when bound to $Tfb1_{PH}$ (17 versus 13 residues). In both complexes, the interface is primarily formed through interactions involving the three hydrophobic amino acids in the ΦXXΦΦ motif present in the α-helix. Mutation of any of the three key residues from the motif, in particular F542, leads to a decrease in binding affinity toward $Tfb1_{PH}$ and CBP_{KIX}. Taken together with the fact that residues from the ΦXXΦΦ motif form a transient helix in the unbound state, this suggests that this region of $p65_{TA1}$ predisposes it for binding with its target proteins.

The NF-κB-family of proteins plays an important role in controlling the transcription of over 500 human genes, and many of these genes are regulated by the p65–p50 heterodimer. In order for p65–p50 to activate these genes, the TAD of p65 forms protein–protein interactions with several different transcriptional regulatory proteins, including CBP and TFIIH (22,74). One of the keys to activation associated with p65 is the recruitment of CBP, which leads to the subsequent acetylation of select lysine residues on p65 depending on the target gene being activated (5,7). The NMR structure of the $p65_{TA2}$–CBP_{TAZ1} complex is the only other structural information available for the TAD of p65 in complex with a target transcriptional factor (19). Our results demonstrating that $p65_{TA1}$ binds to CBP_{KIX} support that hypothesis that the individual subdomains within the TAD of p65 ($p65_{TA1}$ and $p65_{TA2}$) have the capacity to contact different domains of CBP at the same time, possibly in a cooperative manner. A similar mechanism has been proposed for the interaction of CBP with p53 and FOXO3a (30,68). The TAD of p53 and FOXO3a also both contain two subdomains and each subdomain has a ΦXXΦΦ motif that is important for its binding to CBP. In the case of p53, it has also been shown that its $p53_{TAD1}$ and $p53_{TAD2}$ have the capacity to bind to two domains of CBP when they are artificially fused together (70). The interaction between TFIIH and p65 plays a fundamental role in several processes including the regulation of transcription from the HIV promoter in the viral long terminal repeat (75,76) as well as the expression of nitric oxide synthase from the *Nos*2 gene in macrophages following infections by pathogenic organisms (77). The Tfb1/p62 subunit is targeted by a number of proteins containing an acidic TAD including p65, and our structural studies provide evidence of how the ΦXXΦΦ motif of $p65_{TA1}$ regulates its interaction with $Tfb1_{PH}$. The importance of F542 within the ΦXXΦΦ motif of $p65_{TA1}$ for the formation of both complexes is consistent with the fact that it has been previously identified as essential for p65 to activate transcription (20). The structures of the two complexes explicitly illustrate the importance of this residue, as it is clear that F542 of $p65_{TA1}$ is positioned in a binding cleft in both complexes where it makes crucial contacts with the transcriptional regulator. Taken together with previous structural studies involving $p65_{TA2}$ (19), these studies with $p65_{TA1}$ provide important insights into how the two subdomains within the TAD of p65 incorporate the ΦXXΦΦ motif in order to separately bind to the different transcriptional regulatory factors needed to help control the vast array of genes targeted by the p65–p50 heterodimer.

ACCESSION NUMBERS

^{1}H, ^{13}C and ^{15}N chemical shifts of $Tfb1_{PH}$–$p65_{TA1}$ complex have been deposited in the BioMagResBank (BMRB) under accession number 30243 and associated 3D model structure coordinates have been deposited in the protein data bank (PDB) under the code 5URN. ^{1}H, ^{13}C and ^{15}N chemical shifts of CBP_{KIX}–$p65_{TA1}$ complex have been deposited in the BMRB under accession number 26867 and associated 3D model structure coordinates have been deposited in the PDB under the code 5U4K.

SUPPLEMENTARY DATA

Supplementary Data are available at NAR Online.

ACKNOWLEDGEMENTS

We thank Dr Alanna Schepartz and Dr. Steven Smith for providing the constructs for expression of the KIX domain of CBP.

FUNDING

Canadian Institutes for Health Research [MOP-74739 to J.G.O.]; Natural Sciences and Engineering Research Council of Canada CREATE program Postdoctoral Fellowship (to L.L.); Natural Sciences and Engineering Research Council of Canada; Canada Foundation for Innovation; Québec ministère de la recherche en science et technologie; McGill University. Funding for open access charge: Canadian Institutes for Health Research.

Conflict of interest statement. None declared.

REFERENCES

1. Hayden,M.S., West,A.P. and Ghosh,S. (2006) NF-κB and the immune response. *Oncogene*, **25**, 6758–6780.
2. Hayden,M.S. and Ghosh,S. (2008) Shared principles in NF-κB signaling. *Cell*, **132**, 344–362.
3. Perkins,N.D. (2007) Integrating cell-signalling pathways with NF-κB and IKK function. *Nat. Rev. Mol. Cell Biol.*, **8**, 49–62.

4. Gerondakis,S., Grumont,R., Gugasyan,R., Wong,L., Isomura,I., Ho,W. and Banerjee,A. (2006) Unravelling the complexities of the NF-κB signalling pathway using mouse knockout and transgenic models. *Oncogene*, **25**, 6781–6799.
5. Huang,B., Yang,X.-D., Lamb,A. and Chen,L.-F. (2010) Posttranslational modifications of NF-κB: Another layer of regulation for NF-κB signaling pathway. *Cell. Signal.*, **22**, 1282–1290.
6. Zhong,H., Voll,R.E. and Ghosh,S. (1998) Phosphorylation of NF-κB p65 by PKA stimulates transcriptional activity by promoting a novel bivalent interaction with the coactivator CBP/p300. *Mol. Cell*, **1**, 661–671.
7. Gerritsen,M.E., Williams,A.J., Neish,A.S., Moore,S., Shi,Y. and Collins,T. (1997) CREB-binding protein/p300 are transcriptional coactivators of p65. *Proc. Natl. Acad. Sci. U.S.A.*, **94**, 2927–2932.
8. Wang,D., Westerheide,S.D., Hanson,J.L. and Baldwin,A.S. (2000) Tumor necrosis factor alpha-induced phosphorylation of RelA/p65 on Ser529 is controlled by casein kinase II. *J. Biol. Chem.*, **275**, 32592–32597.
9. Vermeulen,L., De Wilde,G., Notebaert,S., Vanden Berghe,W. and Haegeman,G. (2002) Regulation of the transcriptional activity of the nuclear factor-kappaB p65 subunit. *Biochem. Pharmacol.*, **64**, 963–970.
10. Duran,A., Diaz-Meco,M.T. and Moscat,J. (2003) Essential role of RelA Ser311 phosphorylation by zetaPKC in NF-kappaB transcriptional activation. *EMBO J.*, **22**, 3910–3918.
11. Chen,L.F., Williams,S.A., Mu,Y., Nakano,H., Duerr,J.M., Buckbinder,L. and Greene,W.C. (2005) NF-kB RelA phosphorylation regulates RelA acetylation. *Mol. Cell. Biol.*, **25**, 7966–7975.
12. Buss,H., Handschick,K., Jurrmann,N., Pekkonen,P., Beuerlein,K., Müller,H., Wait,R., Saklatvala,J., Ojala,P.M., Schmitz,M.L. *et al.* (2012) Cyclin-dependent kinase 6 phosphorylates NF-κB P65 at serine 536 and contributes to the regulation of inflammatory gene expression. *PLoS One*, **7**, e51847.
13. Hwang,Y.-J., Lee,E.-W., Song,J., Kim,H.-R., Jun,Y.-C. and Hwang,K.-A. (2013) MafK positively regulates NF-κB activity by enhancing CBP-mediated p65 acetylation. *Sci. Rep.*, **3**, 1–10.
14. Ashburner,B.P., Westerheide,S.D. and Baldwin,A.S. (2001) The p65 (RelA) subunit of NF-kappaB interacts with the histone deacetylase (HDAC) corepressors HDAC1 and HDAC2 to negatively regulate gene expression. *Mol. Cell. Biol.*, **21**, 7065–7077.
15. Chen,F.E., Huang,D.B., Chen,Y.Q. and Ghosh,G. (1998) Crystal structure of the NF-kB p50/p65 heterodimer complexed to DNA. *Nature*, **391**, 410–413.
16. Berkowitz,B., Huang,D.B., Chen-Park,F.E., Sigler,P.B. and Ghosh,G. (2002) The X-ray crystal structure of the NF- B p50{middle dot}p65 heterodimer bound to the interferon—B site. *J. Biol. Chem.*, **277**, 24694–24700.
17. Escalante,C.R., Shen,L., Thanos,D. and Aggarwal,A.K. (2002) Structure of NF-κB p50/p65 Heterodimer Bound to the PRDII DNA Element from the Interferon-β Promoter. *Structure*, **10**, 383–391.
18. Schmitz,M.L. and Baeuerle,P.A. (1991) The p65 subunit is responsible for the strong transcription activating potential of NF-kappa B. *EMBO J.*, **10**, 3805–3817.
19. Mukherjee,S.P., Behar,M., Birnbaum,H.A., Hoffmann,A., Wright,P.E. and Ghosh,G. (2013) Analysis of the RelA:CBP/p300 interaction reveals its involvement in NF-κB-driven transcription. *PLoS Biol.*, **11**, e1001647.
20. Blair,W.S., Bogerd,H.P., Madore,S.J. and Cullen,B.R. (1994) Mutational analysis of the transcription activation domain of RelA: identification of a highly synergistic minimal acidic activation module. *Mol. Cell. Biol.*, **14**, 7226–7234.
21. Schmitz,M.L., Stelzer,G., Altmann,H., Meisterernst,M. and Baeuerle,P.A. (1995) Interaction of the COOH-terminal transactivation domain of p65 NF-kappa B with TATA-binding protein, transcription factor IIB, and coactivators. *J. Biol. Chem.*, **270**, 7219–7226.
22. O'shea,J.M. and Perkins,N.D. (2008) Regulation of the RelA (p65) transactivation domain. *Biochm. Soc. Trans.*, **36**, 603–608.
23. Burkhart,B.A., Hebbar,P.B., Trotter,K.W. and Archer,T.K. (2005) Chromatin-dependent E1A activity modulates NF- B RelA-mediated repression of glucocorticoid receptor-dependent transcription. *J. Biol. Chem.*, **280**, 6349–6358.
24. Schmitz,M.L., dos Santos Silva,M.A., Altmann,H., Czisch,M., Holak,T.A. and Baeuerle,P.A. (1994) Structural and functional analysis of the NF-kappa B p65 C terminus. *J. Biol. Chem.*, **269**, 25613–25620.
25. Lu,H. and Levine,A.J. (1995) Human TAFII31 protein is a transcriptional coactivator of the p53 protein. *Proc. Natl. Acad. Sci. U.S.A.*, **92**, 5154–5158.
26. Buschmann,T., Lin,Y., Aithmitti,N., Fuchs,S.Y., Lu,H., Resnick-Silverman,L., Manfredi,J.J., Ronai,Z. and Wu,X. (2001) Stabilization and activation of p53 by the coactivator protein TAFII31. *J. Biol. Chem.*, **276**, 13852–13857.
27. Di Lello,P., Jenkins,L.M.M., Jones,T.N., Nguyen,B.D., Hara,T., Yamaguchi,H., Dikeakos,J.D., Appella,E., Legault,P. and Omichinski,J.G. (2006) Structure of the Tfb1/p53 complex: insights into the interaction between the p62/Tfb1 subunit of TFIIH and the activation domain of p53. *Mol. Cell*, **22**, 731–740.
28. Teufel,D.P., Freund,S.M., Bycroft,M. and Fersht,A.R. (2007) Four domains of p300 each bind tightly to a sequence spanning both transactivation subdomains of p53. *Proc. Natl. Acad. Sci.*, **104**, 7009–7014.
29. Langlois,C., Mas,C., Di Lello,P., Jenkins,L.M.M., Legault,P. and Omichinski,J.G. (2008) NMR structure of the complex between the Tfb1 subunit of TFIIH and the activation domain of VP16: structural similarities between VP16 and p53. *J. Am. Chem. Soc.*, **130**, 10596–10604.
30. Lee,C.W., Arai,M., Martinez-Yamout,M.A., Dyson,H.J. and Wright,P.E. (2009) Mapping the interactions of the p53 transactivation domain with the KIX domain of CBP †. *Biochemistry*, **48**, 2115–2124.
31. Okuda,M. and Nishimura,Y. (2014) Extended string binding mode of the phosphorylated transactivation domain of tumor suppressor p53. *J. Am. Chem. Soc.*, **136**, 14143–14152.
32. Arai,M., Ferreon,J.C. and Wright,P.E. (2012) Quantitative analysis of multisite protein–ligand interactions by NMR: binding of intrinsically disordered p53 transactivation subdomains with the TAZ2 domain of CBP. *J. Am. Chem. Soc.*, **134**, 3792–3803.
33. Di Lello,P., Nguyen,B.D., Jones,T.N., Potempa,K., Kobor,M.S., Legault,P. and Omichinski,J.G. (2005) NMR structure of the amino-terminal domain from the Tfb1 subunit of TFIIH and characterization of its phosphoinositide and VP16 binding sites †, ‡. *Biochemistry*, **44**, 7678–7686.
34. Langlois,C., Del Gatto,A., Arseneault,G., Lafrance-Vanasse,J., De Simone,M., Morse,T., de Paola,I., Lussier-Price,M., Legault,P., Pedone,C. *et al.* (2012) Structure-based design of a potent artificial transactivation domain based on p53. *J. Am. Chem. Soc.*, **134**, 1715–1723.
35. Muhandiram,D.R. and Kay,L.E. (1994) Gradient-enhanced triple-resonance three-dimensional NMR experiments with improved sensitivity. *J. Magn. Reson. B*, **103**, 203–216.
36. Kay,L.E., Xu,G.Y., Singer,A.U., Muhandiram,D.R. and Formankay,J.D. (1993) A gradient-enhanced HCCH-TOCSY experiment for recording side-chain 1H and 13C correlations in H2O samples of proteins. *J. Magn. Reson. B*, **101**, 333–337.
37. Zhang,O., Kay,L.E., Olivier,J.P. and Forman-Kay,J.D. (1994) Backbone 1H and 15N resonance assignments of the N-terminal SH3 domain of drk in folded and unfolded states using enhanced-sensitivity pulsed field gradient NMR techniques. *J. Biomol. NMR*, **4**, 845–858.
38. Zuiderweg,E.R.P., McIntosh,L.P., Dahlquist,F.W. and Fesik,S.W. (1990) Three-dimensional 13C-resolved protein NOE spectroscopy of uniformly 13C-labeled proteins for the NMR assignment and structure determination of larger molecules. *J. Magn. Reson.*, **86**, 210–216.
39. Zwahlen,C., Legault,P., Vincent,S.J.F., Greenblatt,J., Konrat,R. and Kay,L.E. (1997) Methods for measurement of intermolecular NOEs by multinuclear NMR spectroscopy: application to a bacteriophage λ N-Peptide/ boxBRNA complex. *J. Am. Chem. Soc.*, **119**, 6711–6721.
40. Delaglio,F., Grzesiek,S., Vuister,G.W., Zhu,G., Pfeifer,J. and Bax,A. (1995) NMRPipe: a multidimensional spectral processing system based on UNIX pipes. *J. Biomol. NMR*, **6**, 277–293.
41. Vranken,W.F., Boucher,W., Stevens,T.J., Fogh,R.H., Pajon,A., Llinas,M., Ulrich,E.L., Markley,J.L., Ionides,J. and Laue,E.D. (2005) The CCPN data model for NMR spectroscopy: development of a software pipeline. *Proteins*, **59**, 687–696.

42. Marsh,J.A., Singh,V.K., Jia,Z. and Forman-Kay,J.D. (2006) Sensitivity of secondary structure propensities to sequence differences between α- and γ-synuclein: Implications for fibrillation. *Protein Sci.*, **15**, 2795–2804.
43. Zhang,H., Neal,S. and Wishart,D.S. (2003) RefDB: a database of uniformly referenced protein chemical shifts. *J. Biomol. NMR*, **25**, 173–195.
44. Shen,Y. and Bax,A. (2013) Protein backbone and sidechain torsion angles predicted from NMR chemical shifts using artificial neural networks. *J. Biomol. NMR*, **56**, 227–241.
45. Shen,Y., Delaglio,F., Cornilescu,G. and Bax,A. (2009) TALOS+: a hybrid method for predicting protein backbone torsion angles from NMR chemical shifts. *J. Biomol. NMR*, **44**, 213–223.
46. Habeck,M., Rieping,W., Linge,J.P. and Nilges,M. (2004) NOE assignment with ARIA 2.0: the nuts and bolts. *Methods Mol. Biol.*, **278**, 379–402.
47. Brünger,A.T., Adams,P.D., Clore,G.M., DeLano,W.L., Gros,P., Grosse-Kunstleve,R.W., Jiang,J.S., Kuszewski,J., Nilges,M., Pannu,N.S. *et al.* (1998) Crystallography & NMR system: a new software suite for macromolecular structure determination. *Acta Crystallogr. D Biol. Crystallogr.*, **54**, 905–921.
48. Krieger,E. and Vriend,G. (2014) YASARA View—molecular graphics for all devices—from smartphones to workstations. *Bioinformatics*, **30**, 2981–2982.
49. Krieger,E., Joo,K., Lee,J., Lee,J., Raman,S., Thompson,J., Tyka,M., Baker,D. and Karplus,K. (2009) Improving physical realism, stereochemistry, and side-chain accuracy in homology modeling: four approaches that performed well in CASP8. *Proteins*, **77**(Suppl. 9), 114–122.
50. Canutescu,A.A., Shelenkov,A.A. and Dunbrack,R.L. (2003) A graph-theory algorithm for rapid protein side-chain prediction. *Protein Sci.*, **12**, 2001–2014.
51. Bhattacharya,A., Tejero,R. and Montelione,G.T. (2007) Evaluating protein structures determined by structural genomics consortia. *Proteins*, **66**, 778–795.
52. Gietz,R.D. and Woods,R.A. (2002) Transformation of yeast by lithium acetate/single-stranded carrier DNA/polyethylene glycol method. *Meth. Enzymol.*, **350**, 87–96.
53. Di Lello,P., Jenkins,L.M.M., Mas,C., Langlois,C., Malitskaya,E., Fradet-Turcotte,A., Archambault,J., Legault,P. and Omichinski,J.G. (2008) p53 and TFIIE share a common binding site on the Tfb1/p62 subunit of TFIIH. *Proc. Natl. Acad. Sci. U.S.A.*, **105**, 106–111.
54. Uesugi,M., Nyanguile,O., Lu,H., Levine,A.J. and Verdine,G.L. (1997) Induced alpha helix in the VP16 activation domain upon binding to a human TAF. *Science*, **277**, 1310–1313.
55. De Guzman,R.N., Goto,N.K., Dyson,H.J. and Wright,P.E. (2006) Structural basis for cooperative transcription factor binding to the CBP coactivator. *J. Mol. Biol.*, **355**, 1005–1013.
56. Denis,C.M., Chitayat,S., Plevin,M.J., Wang,F., Thompson,P., Liu,S., Spencer,H.L., Ikura,M., LeBrun,D.P. and Smith,S.P. (2012) Structural basis of CBP/p300 recruitment in leukemia induction by E2A-PBX1. *Blood*, **120**, 3968–3977.
57. Mas,C., Lussier-Price,M., Soni,S., Morse,T., Arseneault,G., Di Lello,P., Lafrance-Vanasse,J., Bieker,J.J. and Omichinski,J.G. (2011) Structural and functional characterization of an atypical activation domain in erythroid Kruppel-like factor (EKLF). *Proc. Natl. Acad. Sci. U.S.A.*, **108**, 10484–10489.
58. Chabot,P.R., Raiola,L., Lussier-Price,M., Morse,T., Arseneault,G., Archambault,J. and Omichinski,J.G. (2014) Structural and functional characterization of a complex between the acidic transactivation domain of EBNA2 and the Tfb1/p62 subunit of TFIIH. *PLoS Pathog.*, **10**, e1004042.
59. Mielke,S.P. and Krishnan,V.V. (2009) Characterization of protein secondary structure from NMR chemical shifts. *Prog. Nucl. Magn. Reson. Spectrosc.*, **54**, 141–165.
60. Goto,N.K., Zor,T., Martinez-Yamout,M., Dyson,H.J. and Wright,P.E. (2002) Cooperativity in transcription factor binding to the coactivator CREB-binding protein (CBP). The mixed lineage leukemia protein (MLL) activation domain binds to an allosteric site on the KIX domain. *J. Biol. Chem.*, **277**, 43168–43174.
61. Brüschweiler,S., Konrat,R. and Tollinger,M. (2013) Allosteric communication in the KIX domain proceeds through dynamic repacking of the hydrophobic core. *ACS Chem. Biol.*, **8**, 1600–1610.
62. Zor,T., De Guzman,R.N., Dyson,H.J. and Wright,P.E. (2004) Solution structure of the KIX domain of CBP bound to the transactivation domain of c-Myb. *J. Mol. Biol.*, **337**, 521–534.
63. Candau,R., Scolnick,D.M., Darpino,P., Ying,C.Y., Halazonetis,T.D. and Berger,S.L. (1997) Two tandem and independent sub-activation domains in the amino terminus of p53 require the adaptor complex for activity. *Oncogene*, **15**, 807–816.
64. Regier,J.L., Shen,F. and Triezenberg,S.J. (1993) Pattern of aromatic and hydrophobic amino acids critical for one of two subdomains of the VP16 transcriptional activator. *Proc. Natl. Acad. Sci. U.S.A.*, **90**, 883–887.
65. So,C.W. and Cleary,M.L. (2002) MLL-AFX requires the transcriptional effector domains of AFX to transform myeloid progenitors and transdominantly interfere with forkhead protein function. *Mol. Cell. Biol.*, **22**, 6542–6552.
66. Chen,X. and Bieker,J.J. (1996) Erythroid Krüppel-like factor (EKLF) contains a multifunctional transcriptional activation domain important for inter- and intramolecular interactions. *EMBO J.*, **15**, 5888–5896.
67. Brzovic,P.S., Heikaus,C.C., Kisselev,L., Vernon,R., Herbig,E., Pacheco,D., Warfield,L., Littlefield,P., Baker,D., Klevit,R.E. *et al.* (2011) The acidic transcription activator Gcn4 binds the mediator subunit Gal11/Med15 using a simple protein interface forming a fuzzy complex. *Mol. Cell*, **44**, 942–953.
68. Wang,F., Marshall,C.B., Yamamoto,K., Li,G.Y., Gasmi-Seabrook,G.M.C., Okada,H., Mak,T.W. and Ikura,M. (2012) Structures of KIX domain of CBP in complex with two FOXO3a transactivation domains reveal promiscuity and plasticity in coactivator recruitment. *Proc. Natl. Acad. Sci. U.S.A.*, **109**, 6078–6083.
69. Radhakrishnan,I., Pérez-Alvarado,G.C., Parker,D., Dyson,H.J., Montminy,M.R. and Wright,P.E. (1997) Solution structure of the KIX domain of CBP bound to the transactivation domain of CREB: a model for activator:coactivator interactions. *Cell*, **91**, 741–752.
70. Krois,A.S., Ferreon,J.C., Martinez-Yamout,M.A., Dyson,H.J. and Wright,P.E. (2016) Recognition of the disordered p53 transactivation domain by the transcriptional adapter zinc finger domains of CREB-binding protein. *Proc. Natl. Acad. Sci. U.S.A.*, **113**, E1853–E1862.
71. De Guzman,R.N., Martinez-Yamout,M.A., Dyson,H.J. and Wright,P.E. (2004) Interaction of the TAZ1 domain of the CREB-binding protein with the activation domain of CITED2: regulation by competition between intrinsically unstructured ligands for non-identical binding sites. *J. Biol. Chem.*, **279**, 3042–3049.
72. Miller Jenkins,L.M., Feng,H., Durell,S.R., Tagad,H.D., Mazur,S.J., Tropea,J.E., Bai,Y. and Appella,E. (2015) Characterization of the p300 Taz2–p53 TAD2 complex and comparison with the p300 Taz2–p53 TAD1 complex. *Biochemistry*, **54**, 2001–2010.
73. Denis,C.M., Langelaan,D.N., Kirlin,A.C., Chitayat,S., Munro,K., Spencer,H.L., LeBrun,D.P. and Smith,S.P. (2014) Functional redundancy between the transcriptional activation domains of E2A is mediated by binding to the KIX domain of CBP/p300. *Nucleic Acids Res.*, **42**, 7370–7382.
74. Näär,A.M., Beaurang,P.A., Zhou,S., Abraham,S., Solomon,W. and Tjian,R. (1999) Composite co-activator ARC mediates chromatin-directed transcriptional activation. *Nature*, **398**, 828–832.
75. West,M.J., Lowe,A.D. and Karn,J. (2001) Activation of human immunodeficiency virus transcription in T cells revisited: NF-kB p65 stimulates transcriptional elongation. *J. Virol.*, **75**, 8524–8537.
76. Kim,Y.K., Bourgeois,C.F., Pearson,R., Tyagi,M., West,M.J., Wong,J., Wu,S.-Y., Chiang,C.-M. and Karn,J. (2006) Recruitment of TFIIH to the HIV LTR is a rate-limiting step in the emergence of HIV from latency. *EMBO J.*, **25**, 3596–3604.
77. Farlik,M., Reutterer,B., Schindler,C., Greten,F., Vogl,C., Müller,M. and Decker,T. (2010) Nonconventional initiation complex assembly by STAT and NF-κB transcription factors regulates nitric oxide synthase expression. *Immunity*, **33**, 25–34.